Loss of endothelial cell-specific autophagy-related protein 7 exacerbates doxorubicin-induced cardiotoxicity

Albert Z. Luu [a,b], Vincent Z. Luu [a,b], Biswajit Chowdhury [a], Andrew Kosmopoulos [a], Yi Pan [a], Mohammed Al-Omran [b,c,d], Adrian Quan [a], Hwee Teoh [a,e], David A. Hess [b,c,f,g], Subodh Verma [a,b,d,*]

[a] Division of Cardiac Surgery, Keenan Research Centre for Biomedical Science of St. Michael's Hospital, Unity Health Toronto, Toronto, Ontario, Canada
[b] Department of Pharmacology and Toxicology, University of Toronto, Toronto, Ontario, Canada
[c] Division of Vascular Surgery, Keenan Research Centre for Biomedical Science of St. Michael's Hospital, Unity Health Toronto, Toronto, Ontario, Canada
[d] Department of Surgery, University of Toronto, Toronto, Ontario, Canada
[e] Division of Endocrinology and Metabolism, Li Ka Shing Knowledge Institute of St. Michael's Hospital, Unity Health Toronto, Toronto, Ontario, Canada
[f] Molecular Medicine Research Laboratories, Krembil Centre for Stem Cell Biology, Robarts Research Institute, Western University, London, Ontario, Canada
[g] Department of Physiology and Pharmacology, Schulich School of Medicine and Dentistry, Western University, London, Ontario, Canada

ARTICLE INFO

ABSTRACT

Doxorubicin (DOX) is an effective, broad-spectrum antineoplastic agent with serious cardiotoxic side effects, which may lead to the development of heart failure. Current strategies to diagnose, prevent, and treat DOX-induced cardiotoxicity (DIC) are inadequate. Recent evidence has linked the dysregulation and destruction of the vascular endothelium to the development of DIC. Autophagy is a conserved pro-survival mechanism that recycles and removes damaged sub-cellular components. Autophagy-related protein 7 (ATG7) catalyzes auto-phagosome formation, a critical step in autophagy. In this study, we used endothelial cell-specific *Atg7* knockout (*EC-Atg7*$^{-/-}$) mice to characterize the role of endothelial cell-specific autophagy in DIC. DOX-treated *EC-Atg7*$^{-/-}$ mice showed reduced survival and a greater decline in cardiac function compared to wild-type controls. His-tological assessments revealed increased cardiac fibrosis in DOX-treated *EC-Atg7*$^{-/-}$ mice. Furthermore, DOX-treated *EC-Atg7*$^{-/-}$ mice had elevated serum levels of creatine kinase-myocardial band, a biomarker for car-diac damage. Thus, the lack of EC-specific autophagy exacerbated DIC. Future studies on the relationship be-tween EC-specific autophagy and DIC could establish the importance of endothelium protection in preventing DIC.

1. Introduction

The anthracycline doxorubicin (DOX) is broadly prescribed to treat solid and hematological cancers, and although effective as a chemo-therapeutic agent, its use has been complicated by both acute and chronic cardiotoxic side effects [1]. The cumulative literature suggests that up to 36% of DOX-treated patients develop cardiomyopathy that may progress to heart failure [2]. Indeed, DOX-induced heart failure has been associated with 50% mortality 1 year following diagnosis [2]. The current options for diagnosing, treating, and preventing DOX-induced cardiotoxicity (DIC) are sub-optimal and highlight the urgency to un-cover the mechanisms that contribute to the development and pro-gression of DIC [3–5]. Earlier studies on DIC tended to focus on the

direct toxic effects of DOX on cardiomyocytes (CMs) [6,7]. Recently, however, there has been a shift in attention toward the vascular endo-thelium as an indirect target of DOX [1]. Endothelial cells (ECs), support optimal CM function by forming physical barriers that prevent the exposure of toxins to CMs. ECs also secrete paracrine factors such as nitric oxide, endothelin-1, prostacyclin, and neuregulin-1, effectors that contribute to CM survival and function [8–12]. Since DOX is adminis-tered intravenously, the ECs that line the vascular lumen are directly exposed to high concentrations of DOX and this may culminate in DOX-induced EC damage thereby preventing endothelium-associated CM protection. Thus, preservation of EC function during DOX therapy may represent a novel therapeutic avenue to help prevent the develop-ment of DIC. The toxic effects that DOX exerts on CMs is similar its

impact on ECs. The major proposed mechanisms include oxidative stress and mitochondria dysfunction, which ultimately leads to cell dysfunction and death [1].

Autophagy, including macroautophagy, microautophagy, and chaperone-mediated autophagy, is a conserved process of cell preservation whereby damaged cellular components are broken down into their basic constituents via lysosomal degradation [13]. Autophagy is tightly regulated by proteins like B-cell lymphoma 2 because excessive degradation can lead to cell death [14]. Macroautophagy, which accounts for the majority of autophagic events, involves the formation of an autophagosome, a double-layer membrane structure, that engulfs cellular content to be degraded [15]. The autophagosome eventually fuses with the lysosome and the contents are subsequently degraded by acid hydrolases [15]. The formation and maturation of the autophagosome require a plethora of proteins such as autophagy-related gene 7 (ATG7), an essential mediator responsible for catalyzing several steps in the autophagosome maturation process [16]. The ATG7 protein is essential for mitophagy and removal of toxic protein aggregates from oxidative stress, which would be important for cell survival and function after DOX exposure [17,18]. We hypothesized that knocking out the *Atg7* gene in ECs would exacerbate DIC. To this end, we report herein the differences in survivability, cardiac function and histology, and levels of creatine kinase-myocardial band (CK-MB) between DOX-treated WT and *EC-Atg7*$^{-/-}$ mice.

2. Materials and methods

2.1. Animals

All procedures adhered to the guidelines of the Canadian Council on Animal Care and were approved by the Institutional Animal Care Committee (protocol 801). *EC-Atg7*$^{-/-}$ mice were generated by crossing the double-floxed Atg7 mouse (*Atg7*$^{flox/flox}$) with the VE-cadherin Cre transgenic (*VE-Cadherin*$^{Cre/}$) mouse (Jackson Laboratory) [19]. All studies were conducted with male mice only. To determine survivability, 8-10-week-old wild-type (WT) and *EC-Atg7*$^{-/-}$ mice were administered either DOX (20 mg/kg) or saline (SAL, 0.9% NaCl) intraperitoneally as a single injection, which has been previously characterized [20]. In the cardiac functional assessment studies, WT and *EC-Atg7*$^{-/-}$ mice underwent baseline echocardiography 2–3 days before treatment with DOX (20 mg/kg) and follow-up echocardiography on Day 3. This timeline was based on survival evaluations. Three days after DOX (20 mg/kg) or SAL (0.9% NaCl) treatment, WT and *EC-Atg7*$^{-/-}$ mice were euthanized and their heart, lung, and serum collected for morphological and molecular analyses.

2.2. Co-immunofluorescence

In order to minimize the number of animals used, lung samples were used to confirm the surrogate mouse model. WT and *EC-Atg7*$^{-/-}$ mice were anesthetized with isoflurane (5%) and euthanized via cervical dislocation. The left lung was isolated and placed in Tissue-Tek® Optimal Cutting Tissue (Sakura) medium-filled cryomolds and 8 μm-thick cryosections were acquired. The sections were incubated with a primary antibody cocktail consisting of anti-rabbit ATG7 (Abcam, Cat# ab133528, 1:500 dilution) and anti-rat cluster of differentiation 31 (CD31) (Abcam, Cat# ab56299, 1:200 dilution). Subsequently, tissue sections were incubated with a secondary antibody cocktail containing goat anti-rabbit Alexa Fluor 555 (Thermo Fisher, Cat#A21428, 1:200 dilution) and goat anti-rat Alexa Fluor 488 (Abcam, Cat#ab150165, 1:200 dilution) before counterstaining with 4′,6-diamidino-2-phenyl-indole (DAPI). The sections were viewed with an Olympus Upright BX150 widefield microscope at 40× magnification. Images of CD31 expression were captured using the red filter cube with 25 ms exposure times. Images of the ATG7 stained sections were captured using a green filter cube with 90 ms exposure times. Images of the nucleus (DAPI

stained) were then captured using a blue filter cube with 4 ms exposure times. All images were taken at a resolution of 4140×3096. The three images of each section were superimposed. Since CD31 is only expressed in EC's, the absence of ATG+ in CD31$^+$ cells validated the *EC-Atg7*$^{-/-}$ mouse model [21].

2.3. Echocardiography assessments

Mice were anesthetized with 2–3% isoflurane via a nose cone. Ultrasound was performed using the Vivo 2100 ultrasound machine and a 40 MHz transducer (VisualSonics). The short-axis motion-mode provided a temporal resolution of the physical and functional aspects of the left ventricle (LV) for each mouse. The transducer was placed transversely along the left chest of each mouse. Images were analyzed using the Vevo LAB 1.7.1 software (VisualSonics). The motion at a segment of the LV wall (anterior epicardium, anterior endocardium, posterior epicardium, posterior endocardium) was used to calculate the functional parameters, LV ejection fraction (EF) and LV fractional shortening (FS).

2.4. Cardiomyocyte vacuolization

Mouse hearts were fixed with 10% neutral buffered formaldehyde for 18–24 h and stored in 70% ethanol. The hearts were processed and embedded in paraffin, and 5 μm thick sections were acquired. To obtain a longitudinal representation of the heart for comparative purposes, three sections were chosen as follows for Hematoxylin and Eosin (H&E) staining and analyses. The first section was the most superficial and was defined as when both cardiac ventricles first became well-defined. The second section was the deepest and was defined as when both cardiac ventricles took up the greatest area. The third section was a section that was located approximately halfway between the first and second. The slides were scanned with the Zeiss Axioscan Scan.Z1 under brightfield settings at 20× magnification. The Zen 2.6 software (Zeiss) was used to view the images. Rectangular boxes were randomly annotated in the LV areas, serving as the areas of interest. A total area of at least 0.7 mm/section (2.4 mm/mouse) was used to quantify the number of vacuoles. Vacuoles were differentiated from tears/rips in the tissue by their circular shape. The average numbers of vacuoles per 1 mm^2 of LV tissue were analyzed.

2.5. Cardiac fibrosis

A section with pronounced cardiac ventricles was chosen to be stained with Masson's Trichrome to semi-quantitatively assess collagen deposition. The slides were viewed under the widefield microscope Olympus Upright BX150 at 40× magnification. The areas of interest included the edges of the heart, left ventricle, and the ventricular lumen. Three images captured these aspects: the edge, the left ventricle, and the area around the LV lumen. Two blinded independent assessors rated the images on a scale of 1–10 based on the extent of collagen deposition, with 10 indicating the greatest amount. The average scores between the two assessors were used for the final analysis.

2.6. Serum CK-MB levels

Enzyme-linked immunosorbent assays (ELISAs) were performed using the serum samples of SAL- and DOX-treated WT and *EC-Atg7*$^{-/-}$ mice to quantify CK-MB levels. Assays were performed in triplicate and according to the manufacturer's protocol (MyBioSource, Cat# MBS705293). Since each sample was assayed in triplicate, one of the readings was eliminated if the coefficient of variation was greater than 10% and if two of the readings were consistently distinct from the third. Statistical analyses were performed using the average of each sample.

2.7. Cardiac apoptosis

Three consecutive sections with pronounced cardiac ventricles were chosen to be stained with cleaved caspase-3 (CC3) to assess the extent of apoptosis. The first section was not incubated with the primary antibody (positive control) and the remaining two were stained with an antibody against CC3. The slides were scanned with the Zeiss Axioscan Scan.Z1 under brightfield settings at 20× magnification. CC3+ cells were only counted if they were also stained with 3,3′-Diaminobenzidine, a nuclear stain.

2.8. Statistical analyses

Survival data were analyzed by the log-rank test on the Kaplan-Meier curves. All other data were analyzed by two-way analysis of variances and the Tukey's test for multiple comparisons. These data are presented as mean ± standard deviation and differences were considered significant if the p value was <0.05.

3. Results

3.1. Knockdown of protein expression in the ECs of EC-Atg7$^{-/-}$ mice

Co-immunofluorescence for CD31 and ATG7 was performed on transverse sections of mouse lungs from WT and *EC-Atg7*$^{-/-}$ mice. While ATG7 staining was abundant in the CD31$^+$ cells of WT mice, ATG7 staining was not detected in the CD31$^+$ cells of *EC-Atg7*$^{-/-}$ mice (Fig. 1). This confirmed the EC-specific deletion of *Atg7* in *EC-Atg7*$^{-/-}$ mice. In alignment with our previous study, there was less CD31 staining in the lung sections from *EC-Atg7*$^{-/-}$ mice [22]. CD31$^+$ non-ECs in WT mice could be stem- or progenitor-cells [23].
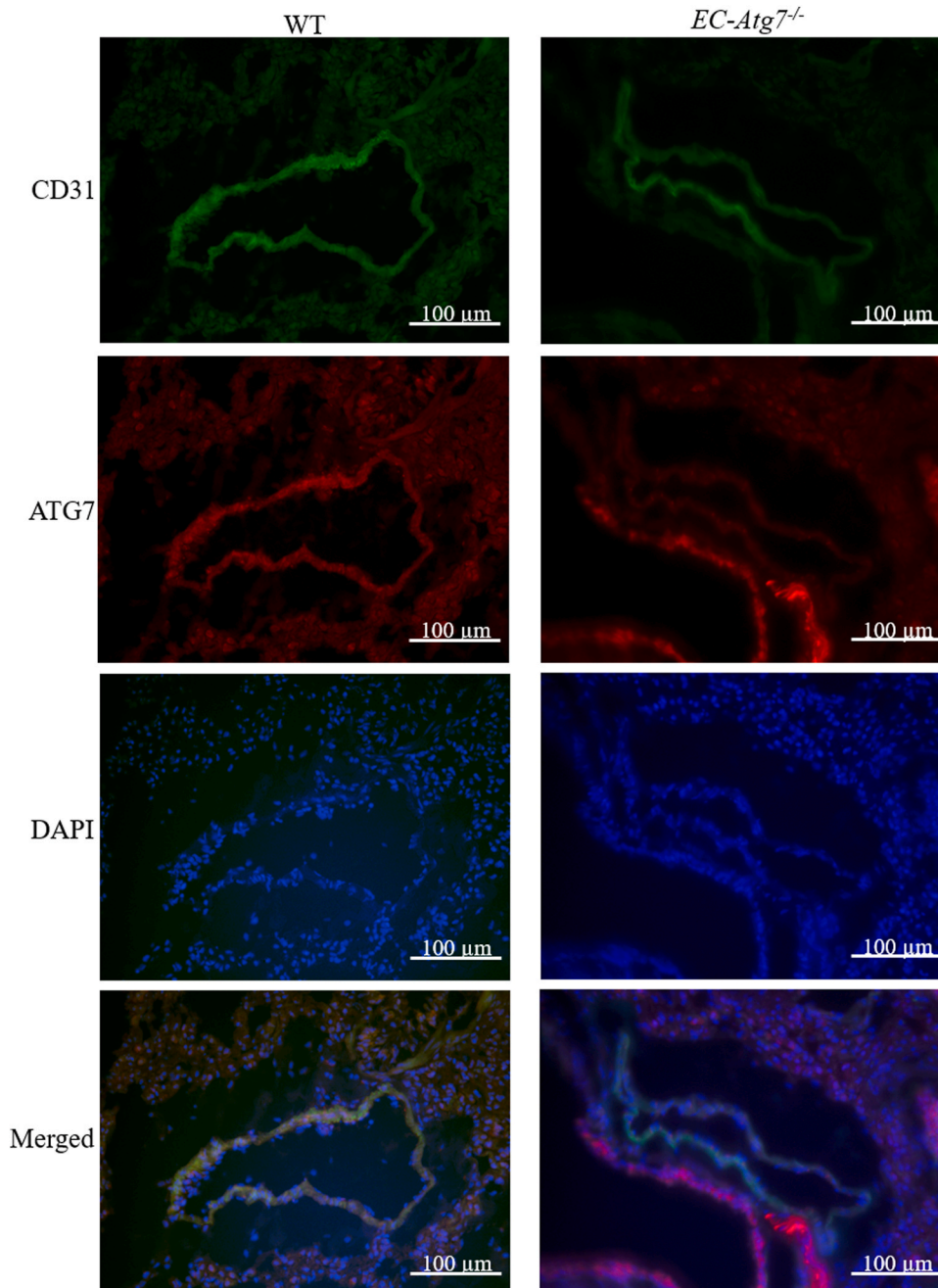
Fig. 1. Loss of ATG7 protein expression in lung ECs of *EC-Atg7*$^{-/-}$ mice. Representative co-immunofluorescence images of the lung sections (transverse) for WT (left) and *EC-Atg7*$^{-/-}$ (right) mice. CD31 (green), ATG7 (red), and 4′,6-diamidino-2-phenylindole (DAPI) (blue) were simultaneously detected (top to bottom). ATG7 was detected in CD31$^+$ cells of WT mice. In contrast, ATG7 was not detected in CD31$^+$ cells from *EC-Atg7*$^{-/-}$ mice. (For interpretation of the references to colour in this figure legend, the reader is referred to the Web version of this article.)

3.2. Reduced survival in DOX-treated EC-Atg7⁻/⁻ mice

Survival was monitored following initiation of DOX treatment (Fig. 2A). The survivability of DOX-treated *EC-Atg7⁻/⁻* mice (3.5 days ±1.6 days, n = 11) was significantly lower than DOX-treated WT mice (5.1 days ±2.1 days, n = 14) (p < 0.05). A 100% survival at the 4-week time point was noted for the SAL-treated WT (n = 10) and *EC-Atg7⁻/⁻* (n = 10) mice. To the best of our knowledge, this is the first study to show that deficiency in EC-specific autophagy increased DOX-associated mortality.

3.3. Reduced cardiac function in DOX-treated EC-Atg7⁻/⁻ mice

Mice underwent ultrasound echocardiography at baseline and Day 3 post-DOX administration to assess changes in cardiac function as defined by LVEF and LVFS. At baseline, there were no differences in LVEF (Fig. 2B) and LVFS (Fig. 2C) measurements between the WT (EF = 75.3% ± 2.7%, FS = 43.2% ± 2.4%, n = 9) and *EC-Atg7⁻/⁻* (EF = 74.7% ± 3.2%, FS = 43.1% ± 2.5%, n = 9) mice. At 3 days post-DOX treatment, LVEF and LVFS were lower in both WT (EF = 69.7% ± 3.2%, p < 0.05; FS = 37.8% ± 2.6%, p < 0.05 compared to baseline) and *EC-Atg7⁻/⁻* mice (EF = 63.8% ± 2.6%, p < 0.05; FS = 33.4% ± 1.3%, p < 0.05 compared to baseline). Notably, the reductions in LVEF and LVFS were less severe in the DOX-treated WT mice (EF = 5.7% ± 4.9%, FS = 5.4% ± 4.1%) when compared to the DOX-treated *EC-Atg7⁻/⁻* mice (EF = 11.0% ± 4.3%, FS = 9.7% ± 2.8%) (p < 0.05). Thus, *Atg7* knockout in ECs exacerbated the decline in cardiac function after DOX-treatment, and this may partially account for the increased mortality observed

among the DOX-treated *EC-Atg7⁻/⁻* mice.

3.4. Increased cardiomyocyte vacuolization after DOX treatment

DOX-mediated CM damage manifests as the loss of myofibers followed by the distension of sacrotubules that lead to vacuole formation [24]. Degenerative LV vacuolization was assessed using H&E-stained paraffinized heart sections from WT and *EC-Atg7⁻/⁻* mice (Fig. 3). Vacuolization was rarely observed in the sections from SAL-treated WT (8.5 ± 1.9 vacuoles/mm², n = 5) and *EC-Atg7⁻/⁻* (8.1 ± 1.9 vacuoles/mm², n = 5) mice. Conversely, sections from DOX-treated WT (22.0 ± 2.8 vacuoles/mm², n = 5) and *EC-Atg7⁻/⁻* (26.7 ± 14.0 vacuoles/mm², n = 5) mice had significantly greater degenerative vacuolization relative to the sections from the corresponding SAL-treated control groups (p < 0.05), suggesting that intensive CM damage had occurred in the DOX-treated mice. This is consistent with the available literature demonstrating that DOX-treatment induces CM vacuolization [20]. The mean number of vacuoles observed in the LV of DOX-treated WT and *EC-Atg7⁻/⁻* mice were comparable, suggesting that the decline in cardiac function documented in the DOX-treated *EC-Atg7⁻/⁻* mice was not associated with an increase in LV vacuolization.

3.5. Increased cardiac fibrosis in DOX-treated EC-Atg7⁻/⁻ mice

The invasion of cardiac fibroblasts into areas with CM toxicity is a process that normally acts to preserve the structural integrity of the heart [25]. This remodeling process can also promote an unfavorable environment for neighboring CMs through the secretion of paracrine
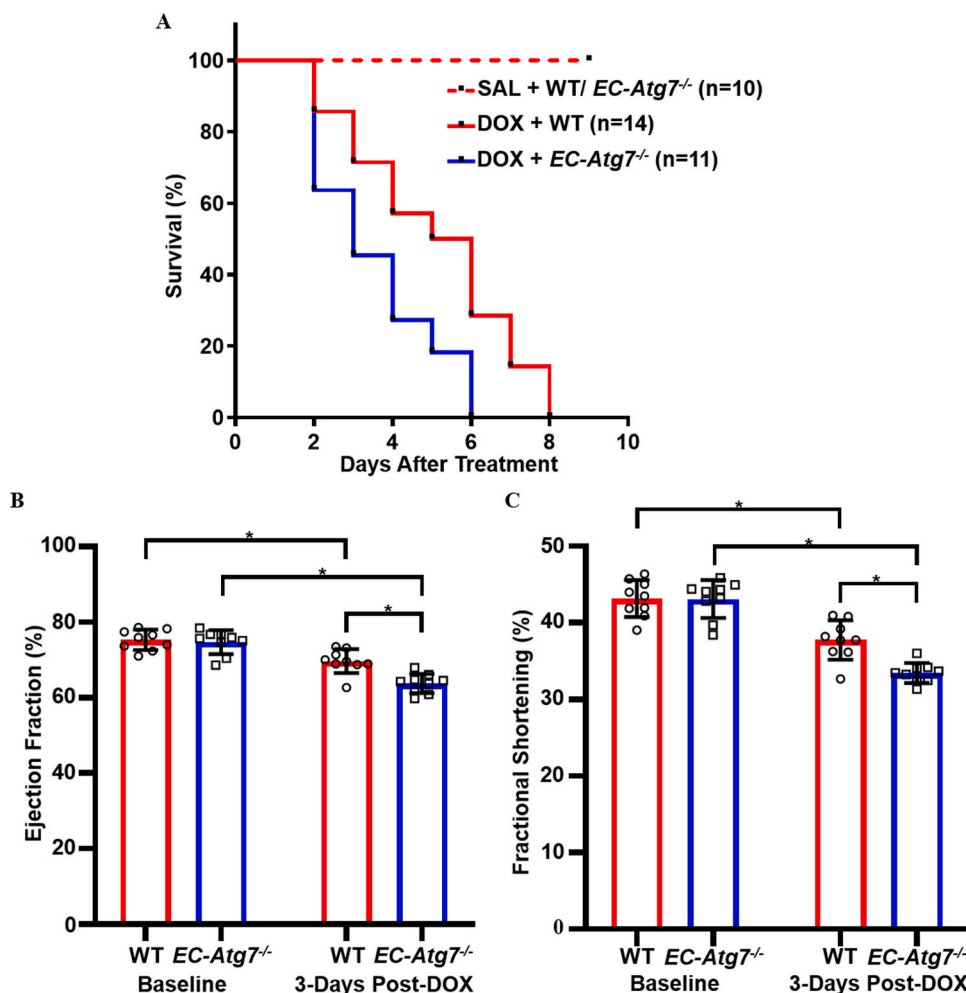
Fig. 2. Reduced survival and cardiac function in DOX-treated *EC-Atg7⁻/⁻* mice. (A) Kaplan-Meier survival curves for WT and *EC-Atg7⁻/⁻* mice after DOX (20 mg/kg) treatment. WT mice survived longer than *EC-Atg7⁻/⁻* mice (p < 0.05 using the log-rank test). (B) Left ventricular ejection fraction (LVEF) and (C) Left ventricular fractional shortening (LVFS) in WT (n = 9) and *EC-Atg7⁻/⁻* (n = 9) mice at baseline and 3 days post-DOX treatment. DOX-treated *EC-Atg7⁻/⁻* mice had reduced LVEF and LVFS compared to their WT littermates. Data are presented as mean ± SD. *p < 0.05 using two-way ANOVA and the Tukey test.

A

B
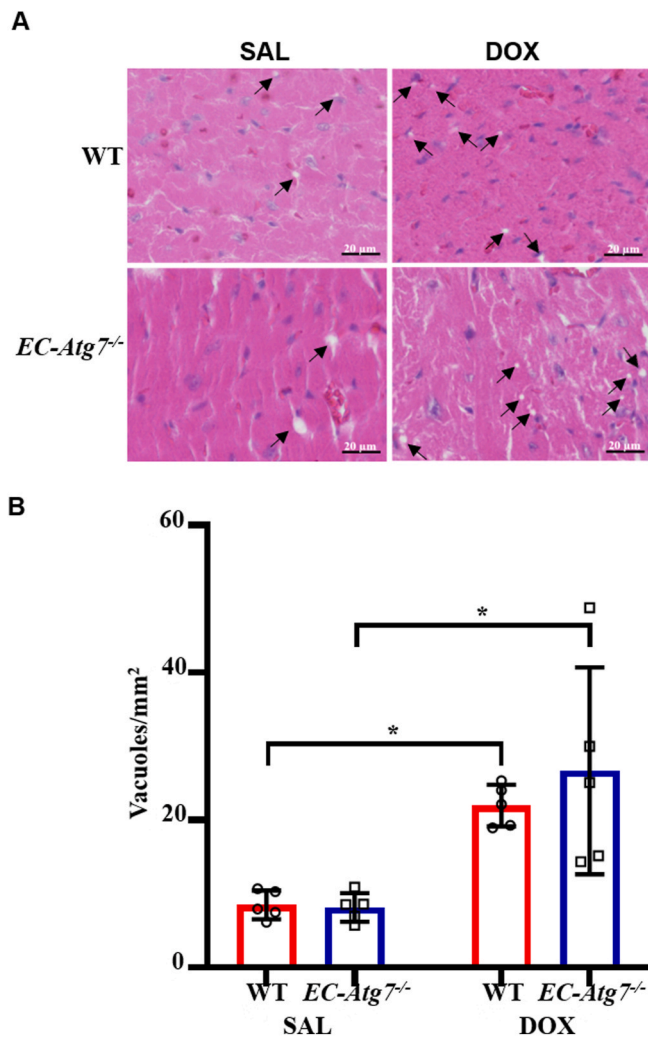
Fig. 3. DOX-treated mice demonstrated increased cardiomyocyte vacuolization. (A) Representative hematoxylin and eosin (H&E) images showing the left ventricles (LV) of WT (top) and *EC-Atg7$^{-/-}$* (bottom) mice three days after SAL (0.9% NaCl) (left) or DOX (20 mg/kg) (right) treatment. The pink and blue areas represent the cytoplasm and nucleus, respectively. (B) Quantification of vacuole number in the LV of WT and *EC-Atg7$^{-/-}$* mice (3 slides/mouse) three days after SAL (n = 5/group) or DOX (n = 5/group) treatment. DOX-treated mice showed increased vacuoles compared to SAL-treated mice. There was no difference in the total number of vacuoles observed between DOX-treated WT and *EC-Atg7$^{-/-}$* mice. Data are presented as mean ± SD. *p < 0.05 using two-way ANOVA followed by Tukey's multiple comparison tests. (For interpretation of the references to colour in this figure legend, the reader is referred to the Web version of this article.)

factors and may exacerbate cardiac damage [26]. LV fibrosis was assessed using Masson's Trichrome-stained heart sections to detect collagen deposition secreted from activated cardiac fibroblasts (Fig. 4A and B). Collagen deposition was minimal in the sections from WT (3.4 ± 0.6, n = 5) and *EC-Atg7$^{-/-}$* (3.3 ± 0.9, n = 5) mice that had undergone SAL treatment. Collagen deposition was significantly greater in the sections from DOX-treated WT (5.2 ± 0.8, p < 0.05) and *EC-Atg7$^{-/-}$* (6.9 ± 1.2, p < 0.05) mice. These findings are consistent with previous rodent studies that reported increased cardiac fibrosis after DOX treatment [20,27]. Furthermore, DOX-treated *EC-Atg7$^{-/-}$* mice showed significantly greater collagen deposition compared to DOX-treated WT mice (p < 0.05), suggesting that an increase in fibrosis may have contributed to reduced cardiac function in DOX-treated *EC-Atg7$^{-/-}$* mice.

3.6. Increased serum CK-MB in DOX-treated EC-Atg7$^{-/-}$ mice

CK-MB is an enzyme that enters the circulation following CM rupture that is triggered by cardiac damage [28]. ELISA assays were performed on the sera of SAL- and DOX-treated WT and *EC-Atg7$^{-/-}$* mice (Fig. 4C). Sera from DOX-treated WT (1971.6 U/I ± 976.3 U/I, n = 5) and *EC-Atg7$^{-/-}$* (4150.9 U/I ± 1879.5 U/I, n = 5) mice had higher CK-MB levels compared to those from SAL-treated WT (192.0 U/I ± 82.6 U/I, n = 6) and *EC-Atg7$^{-/-}$* (292.6 U/I ± 130.9 U/I, n = 5) mice (p < 0.05). This finding is consistent with those of other groups that observed elevated serum CK-MB levels following DOX treatment in mice [20,29]. Additionally, the serum CK-MB levels of DOX-treated *EC-Atg7$^{-/-}$* mice were higher relative to those of DOX-treated WT mice (p < 0.05). This provides additional evidence that DIC was elevated in *EC-Atg7$^{-/-}$* mice.

4. Discussion

Autophagy is a tightly regulated cellular process important for tissue homeostasis and function, especially after DOX exposure. The normalization of autophagy, which becomes dysfunction because of DOX, is a cardioprotective mechanism of metformin for individuals receiving DOX [30].

Due to difficulties with culturing ECs from *EC-Atg7$^{-/-}$* mice, we were unable to quantify the efficiency of *Atg7* deletion in these cells. We observed greater DOX-associated mortality in *EC-Atg7$^{-/-}$* mice compared to their WT counterparts. A previous study observed an increase in DOX-associated mortality in mice that were whole-body knockouts for *Uvrag*, another gene that is essential for autophagosome formation [20]. Our study demonstrated that the loss of endothelial *Atg7* significantly exacerbated DOX-associated mortality in mice. We searched for evidence of increased direct cardiotoxicity and observed a greater decline in LVEF and LVFS in DOX-treated *EC-Atg7$^{-/-}$* mice compared to DOX-treated WT controls. To characterize the changes in cardiac function that may occur in parallel with modifications in cardiac morphology, and to explore potential mechanisms that may contribute to changes in cardiac function, we first assessed CM damage/degeneration via quantification of CM vacuolization. Although DOX-treated WT and *EC-Atg7$^{-/-}$* mice had increased vacuolization compared to SAL-treated control mice, there was no difference in vacuolization between DOX-treated *EC-Atg7$^{-/-}$* and DOX-treated WT mice. It should be noted that vacuoles can only be quantified in cells that are present within the paraffin sections. Significantly damaged CMs with vacuolization in *EC-Atg7$^{-/-}$* mice may have undergone cell death by day 3, indicating that CM vacuole quantification may not reflect the full extent of DOX-induced cardiac damage. However, there were no significant CC3 staining, an apoptotic marker, in the cardiac sections of *EC-Atg7$^{-/-}$* mice (Supplementary Fig. 1). Exaggerated toxicity of DOX in these mice may lead to rapid necrotic death of CMs [31]. We observed greater LV fibrosis in DOX-treated *EC-Atg7$^{-/-}$* mice compared to DOX-WT mice. Cardiac fibrosis has often been associated with systolic and diastolic dysfunction because of its detrimental effects on CMs [32]. Finally, to obtain additional evidence that indicate acute cardiac damage, we assessed serum levels of CK-MB, an enzyme important for energy homeostasis by generating energy buffers in cardiac muscles [28]. *EC-Atg7$^{-/-}$* mice demonstrated higher CK-MB levels compared to WT mice after DOX treatment. This is in congruence with our survival, cardiac functional, and cardiac morphological data, which suggests greater DIC in *EC-Atg7$^{-/-}$* mice compared to their WT littermates.

There are several limitations to this study. Firstly, non-ATG7-dependent autophagic processes such as microautophagy and chaperone-mediated autophagy account for a small but relevant proportion of autophagic events. Thus, autophagy in the ECs of the *EC-Atg7$^{-/-}$* mice we studied were likely reduced, not absent. In addition, microautophagy and chaperone-mediated autophagy, like macroautophagy, has also been observed to remove damaged and oxidized molecules, which can be induced by DOX [33]. Studies examining the
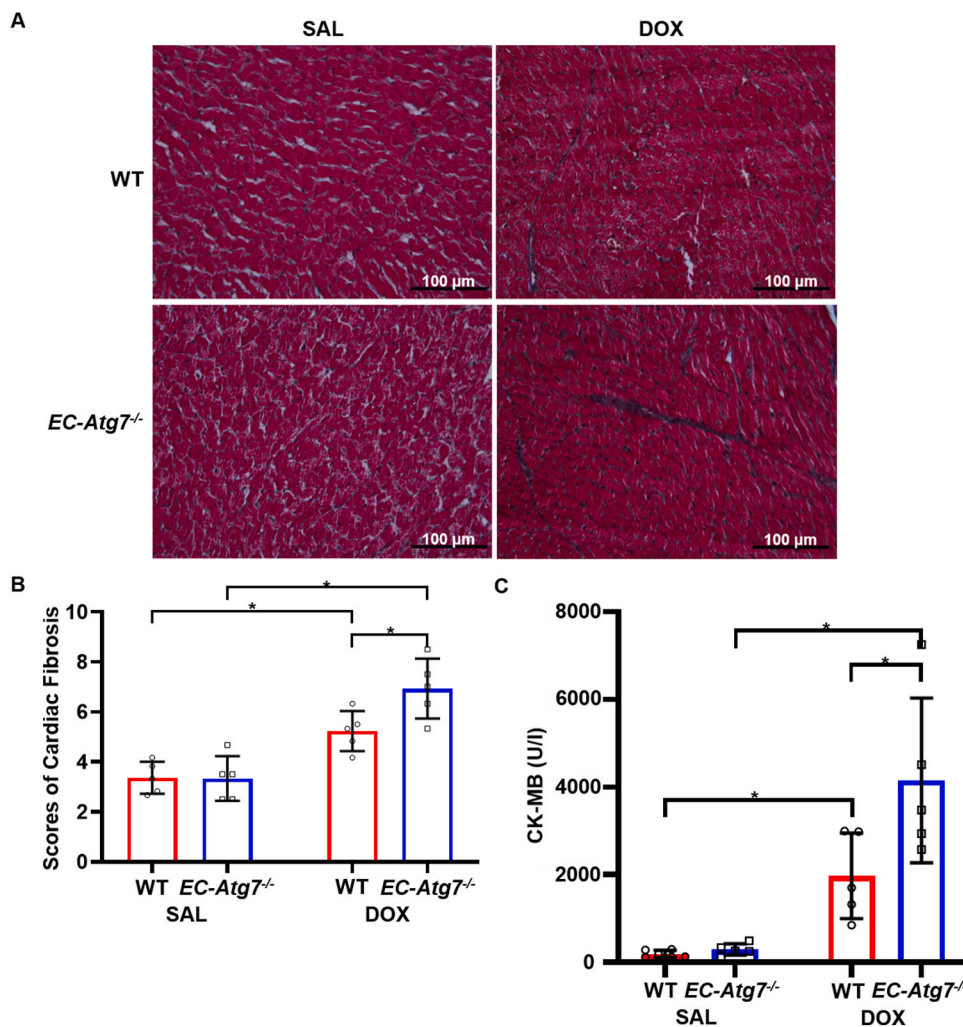
Fig. 4. DOX-treated *EC-Atg7$^{-/-}$* mice demonstrated increased cardiac fibrosis and serum CK-MB. (A) Representative images showing the left ventricle (LV) from WT (top) and *EC-Atg7$^{-/-}$* (bottom) mice stained with Masson's trichrome at 3 days after SAL (0.9% NaCl) (left) or DOX (20 mg/kg) (right) treatment. The dark-blue and red areas represent collagen deposition and the cell cytoplasm, respectively. (B) Blinded scoring of cardiac fibrosis though semi-quantification of the extent of collagen deposition in the LV of WT and *EC-Atg7$^{-/-}$* mice (1 slide/mouse) three days after SAL (n = 5/group) or DOX (n = 5/group) treatment. DOX-treated mice showed increased cardiac fibrosis compared to SAL-treated animals. In addition, DOX-treated *EC-Atg7$^{-/-}$* mice demonstrated increased cardiac fibrosis compared to DOX-treated WT mice. (C) CK-MB levels in the sera of SAL- or DOX-treated WT (n = 5) and *EC-Atg7$^{-/-}$* (n = 5) mice were measured by ELISA assays. DOX-treated *EC-Atg7$^{-/-}$* mice demonstrated increased serum CK-MB compared to DOX-treated WT mice. Data are mean ± SD. *$p < 0.05$ using two-way ANOVA and the Tukey test. (For interpretation of the references to colour in this figure legend, the reader is referred to the Web version of this article.)

extent of autophagic compensation by microautophagy and chaperone-mediated autophagy in the *EC-Atg7$^{-/-}$* mouse model are warranted. Secondly, high-dose DOX delivered intraperitoneally can be toxic towards organs such as the liver, kidney, and intestines, with damage at these sites potentially contributing to DOX-associated mortality [34]. In particular, DOX-mediated intestinal release of endotoxin into the circulation and the subsequent immune response can lead to sepsis and rapid death [35]. Knocking out *Atg7* in ECs, a major component of the vascular system, may lead to endothelium dysfunction and exacerbate sepsis. Serial echocardiography which provides real-time recordings of cardiac function would afford a more accurate description of the temporal impact of cardiac damage in DOX-associated mortality. Thirdly, our study only explored acute DOX cardiotoxicity. Cardiotoxicity due to chronic DOX exposure continues to be a major clinical challenge because it is difficult to detect in its early stages and can become irreversible, potentially developing into heart failure [5]. The induction of acute cardiotoxicity within 3 days of DOX administration limits the breadth of conclusions applicable to our study. Finally, questions remain regarding the molecular mechanisms by which knocking out *Atg7* in ECs seems to accelerate DIC in the *EC-Atg7$^{-/-}$* mouse model. Assessing the changes in EC-CM interactions after the deletion of EC-specific *Atg7* may help elucidate these mechanisms.

In summary, our study provides evidence that the lack of EC-specific autophagy can heighten DIC. Mechanistic investigations on the relationship between EC-specific autophagy and DIC are warranted to establish the importance of endothelium protection in preventing cardiac damage in patients treated with DOX.

CRediT authorship contribution statement

Albert Z. Luu: Conceptualization, Methodology, Validation, Formal analysis, Investigation, Writing - original draft, Writing - review & editing, Visualization. **Vincent Z. Luu:** Methodology, Validation, Formal analysis, Investigation, Writing - review & editing, Visualization. **Biswajit Chowdhury:** Methodology, Validation, Formal analysis, Investigation, Visualization. **Andrew Kosmopoulos:** Investigation, Visualization. **Yi Pan:** Methodology, Validation, Formal analysis, Investigation. **Mohammed Al-Omran:** Resources, Writing - review & editing. **Adrian Quan:** Methodology, Validation, Project administration. **Hwee Teoh:** Writing - original draft, Writing - review & editing, Visualization. **David A. Hess:** Conceptualization, Writing - original draft, Writing - review & editing, Supervision. **Subodh Verma:** Conceptualization, Writing - review & editing, Supervision, Funding acquisition.

Declaration of competing interest

The authors have no relevant conflicts of interest to declare.

Appendix A. Supplementary data

Supplementary data to this article can be found online at https://doi.org/10.1016/j.bbrep.2021.100926.

References

[1] A.Z. Luu, B. Chowdhury, M. Al-Omran, H. Teoh, D.A. Hess, S. Verma, Role of endothelium in doxorubicin-induced cardiomyopathy, JACC. Basic to Transl. Sci. 3 (2018) 861–870, https://doi.org/10.1016/j.jacbts.2018.06.005.

[2] D.D. Von Hoff, M.W. Layard, P. Basa, H.L. Davis Jr., A.L. Von Hoff, M. Rozencweig, F.M. Muggia, Risk factors for doxorubicin-induced congestive heart failure, Ann. Intern. Med. 91 (1979) 710–717.

[3] A.M. Rahman, S.W. Yusuf, M.S. Ewer, Anthracycline-induced cardiotoxicity and the cardiac-sparing effect of liposomal formulation, Int. J. Nanomed. 2 (2007) 567–583.

[4] M.A. Mitry, J.G. Edwards, Doxorubicin induced heart failure: phenotype and molecular mechanisms, Int J Cardiol Hear. Vasc. 10 (2016) 17–24, https://doi.org/10.1016/j.ijcha.2015.11.004.

[5] K. Chatterjee, J. Zhang, N. Honbo, J.S. Karliner, Doxorubicin cardiomyopathy, Cardiology 115 (2010) 155–162, https://doi.org/10.1159/000265166.

[6] A.C. Childs, S.L. Phaneuf, A.J. Dirks, T. Phillips, C. Leeuwenburgh, Doxorubicin treatment in vivo causes cytochrome C release and cardiomyocyte apoptosis, as well as increased mitochondrial efficiency, superoxide dismutase activity, and Bcl-2:Bax ratio, Canc. Res. 62 (2002) 4592–4598.

[7] L.E. Solem, L.J. Heller, K.B. Wallace, Dose-dependent increase in sensitivity to calcium-induced mitochondrial dysfunction and cardiomyocyte cell injury by doxorubicin, J. Mol. Cell. Cardiol. 28 (1996) 1023–1032, https://doi.org/10.1006/jmcc.1996.0095.

[8] E.L. Wilkinson, J.E. Sidaway, M.J. Cross, Cardiotoxic drugs Herceptin and doxorubicin inhibit cardiac microvascular endothelial cell barrier formation resulting in increased drug permeability, Biol Open 5 (2016) 1362–1370, https://doi.org/10.1242/bio.020362.

[9] M. Seddon, A.M. Shah, B. Casadei, Cardiomyocytes as effectors of nitric oxide signalling, Cardiovasc. Res. 75 (2007) 315–326, https://doi.org/10.1016/j.cardiores.2007.04.031.

[10] M. Yanagisawa, H. Kurihara, S. Kimura, Y. Tomobe, M. Kobayashi, Y. Mitsui, Y. Yazaki, K. Goto, T. Masaki, A novel potent vasoconstrictor peptide produced by vascular endothelial cells, Nature 332 (1988) 411–415, https://doi.org/10.1038/332411a0.

[11] E. Ricciotti, G.A. FitzGerald, Prostaglandins and inflammation, Arterioscler. Thromb. Vasc. Biol. 31 (2011) 986–1000, https://doi.org/10.1161/ATVBAHA.110.207449.

[12] S.L. Lim, C.S. Lam, V.F. Segers, D.L. Brutsaert, G.W. De Keulenaer, Cardiac endothelium-myocyte interaction: clinical opportunities for new heart failure therapies regardless of ejection fraction, Eur. Heart J. 36 (2015) 2050–2060, https://doi.org/10.1093/eurheartj/ehv132.

[13] D. Glick, S. Barth, K.F. Macleod, Autophagy: cellular and molecular mechanisms, J. Pathol. 221 (2010) 3–12, https://doi.org/10.1002/path.2697.

[14] S. Pattingre, A. Tassa, X. Qu, R. Garuti, X.H. Liang, N. Mizushima, M. Packer, M. D. Schneider, B. Levine, Bcl-2 antiapoptotic proteins inhibit Beclin 1-dependent autophagy, Cell 122 (2005) 927–939, https://doi.org/10.1016/j.cell.2005.07.002.

[15] Y. Feng, D. He, Z. Yao, D.J. Klionsky, The machinery of macroautophagy, Cell Res. 24 (2014) 24–41, https://doi.org/10.1038/cr.2013.168.

[16] Z. Yin, Y. Zhao, H. Li, M. Yan, L. Zhou, C. Chen, D.W. Wang, miR-320a mediates doxorubicin-induced cardiotoxicity by targeting VEGF signal pathway, Aging 8 (2016) 192–207, https://doi.org/10.18632/aging.100876.

[17] Y. 17, W.-C. Chiang, R.J. Sumpter, P. Mishra, B. Levine, Prohibitin 2 is an inner mitochondrial membrane mitophagy receptor, Cell 168 (2017) 224–238, https://doi.org/10.1016/j.cell.2016.11.042, e10.

[18] I. Lekli, D.D. Haines, G. Balla, A. Tosaki, Autophagy: an adaptive physiological countermeasure to cellular senescence and ischaemia/reperfusion-associated cardiac arrhythmias, J. Cell Mol. Med. 21 (2017) 1058–1072, https://doi.org/10.1111/jcmm.13053.

[19] T. Torisu, K. Torisu, I.H. Lee, J. Liu, D. Malide, C.A. Combs, X.S. Wu, I.I. Rovira, M. M. Fergusson, R. Weigert, P.S. Connelly, M.P. Daniels, M. Komatsu, L. Cao, T. Finkel, Autophagy regulates endothelial cell processing, maturation and secretion of von Willebrand factor, Nat. Med. 19 (2013) 1281–1287, https://doi.org/10.1038/nm.3288.

[20] L. An, X.-W. Hu, S. Zhang, X. Hu, Z. Song, A. Naz, Z. Zi, J. Wu, C. Li, Y. Zou, L. He, H. Zhu, UVRAG deficiency exacerbates doxorubicin-induced cardiotoxicity, Sci. Rep. 7 (2017) 43251, https://doi.org/10.1038/srep43251.

[21] E. Dejana, M. Corada, M.G. Lampugnani, Endothelial cell-to-cell junctions, FASEB J. Off. Publ. Fed. Am. Soc. Exp. Biol. 9 (1995) 910–918.

[22] K.K. Singh, F. Lovren, Y. Pan, A. Quan, A. Ramadan, P.N. Matkar, M. Ehsan, P. Sandhu, L.E. Mantella, N. Gupta, H. Teoh, M. Parotto, A. Tabuchi, W.M. Kuebler, M. Al-Omran, T. Finkel, S. Verma, The essential autophagy gene ATG7 modulates organ fibrosis via regulation of endothelial-to-mesenchymal transition, J. Biol. Chem. 290 (2015) 2547–2559, https://doi.org/10.1074/jbc.M114.604603.

[23] Y. Xu, P. Sun, J.-Y. Wang, Z.-Z. Li, R.-L. Gao, X.-Z. Wang, W.D. Phillips, S.X. Liang, Differentiation of CD45-/CD31+ lung side population cells into endothelial and smooth muscle cells in vitro, Int. J. Mol. Med. 43 (2019) 1128–1138, https://doi.org/10.3892/ijmm.2019.4053.

[24] E.A. Lefrak, J. Pitha, S. Rosenheim, J.A. Gottlieb, A clinicopathologic analysis of adriamycin cardiotoxicity, Cancer 32 (1973) 302–314.

[25] J.G. Travers, F.A. Kamal, J. Robbins, K.E. Yutzey, B.C. Blaxall, Cardiac fibrosis: the fibroblast awakens, Circ. Res. 118 (2016) 1021–1040, https://doi.org/10.1161/CIRCRESAHA.115.306565.

[26] M.O. Gray, C.S. Long, J.E. Kalinyak, H.T. Li, J.S. Karliner, Angiotensin II stimulates cardiac myocyte hypertrophy via paracrine release of TGF-beta 1 and endothelin-1 from fibroblasts, Cardiovasc. Res. 40 (1998) 352–363, https://doi.org/10.1016/s0008-6363(98)00121-7.

[27] X.M. Pei, B.Y. Yung, S.P. Yip, M. Ying, I.F. Benzie, P.M. Siu, Desacyl ghrelin prevents doxorubicin-induced myocardial fibrosis and apoptosis via the GHSR-independent pathway, Am. J. Physiol. Endocrinol. Metab. 306 (2014) E311–E323, https://doi.org/10.1152/ajpendo.00123.2013.

[28] S. Aydin, K. Ugur, S. Aydin, İ. Sahin, M. Yardim, Biomarkers in acute myocardial infarction: current perspectives, Vasc. Health Risk Manag. 15 (2019) 1–10, https://doi.org/10.2147/VHRM.S166157.

[29] S.H. Kim, K.-J. Kim, J.-H. Kim, J.-H. Kwak, H. Song, J.-Y. Cho, D.Y. Hwang, K. S. Kim, Y.-S. Jung, Comparision of doxorubicin-induced cardiotoxicity in the ICR mice of different sources, Lab. Anim. Res. 33 (2017) 165–170, https://doi.org/10.5625/lar.2017.33.2.165.

[30] R. Zilinyi, A. Czompa, A. Czegledi, A. Gajtko, D. Pituk, I. Lekli, A. Tosaki, The cardioprotective effect of metformin in doxorubicin-induced cardiotoxicity: the role of autophagy, Molecules 23 (2018), https://doi.org/10.3390/molecules23051184.

[31] Y.-W. Zhang, J. Shi, Y.-J. Li, L. Wei, Cardiomyocyte death in doxorubicin-induced cardiotoxicity, Arch. Immunol. Ther. Exp. 57 (2009) 435–445, https://doi.org/10.1007/s00005-009-0051-8.

[32] P. Kong, P. Christia, N.G. Frangogiannis, The pathogenesis of cardiac fibrosis, Cell. Mol. Life Sci. 71 (2014) 549–574, https://doi.org/10.1007/s00018-013-1349-6.

[33] I.E. Alfaro, A. Albornoz, A. Molina, J. Moreno, K. Cordero, A. Criollo, M. Budini, Chaperone mediated autophagy in the crosstalk of neurodegenerative diseases and metabolic disorders, Front. Endocrinol. 9 (2018) 778, https://doi.org/10.3389/fendo.2018.00778.

[34] A. Pugazhendhi, T.N.J.I. Edison, B.K. Velmurugan, J.A. Jacob, I. Karuppusamy, Toxicity of Doxorubicin (Dox) to different experimental organ systems, Life Sci. 200 (2018) 26–30, https://doi.org/10.1016/j.lfs.2018.03.023.

[35] H. Xiao, J. Siddiqui, D.G. Remick, Mechanisms of mortality in early and late sepsis, Infect. Immun. 74 (2006) 5227–5235, https://doi.org/10.1128/IAI.01220-05.